THE ASTROPHYSICAL JOURNAL, 325:828–836, 1988 February 15

WHAT DOES AN ERUPTING NOVA DO TO ITS RED DWARF COMPANION?

ATTAY KOVETZ
Tel Aviv University

DINA PRIALNIK
Hebrew University and Tel Aviv University

AND

MICHAEL M. SHARA
Space Telescope Science Institute

Received 1987 April 23; accepted 1987 July 30

ABSTRACT

During nova eruptions and for decades afterward, the red dwarfs in cataclysmic binaries are irradiated with hundreds of times more luminosity than they themselves produce. Simulations of the time-dependent irradiation of three red dwarf models (0.25, 0.50, and 0.75 $M_\odot$) are presented. The mass transfer rates forced by irradiation after nova eruption are found to be enhanced by two orders of magnitude because of the irradiation. The time scale for irradiation to become unimportant is that of the white dwarf cooling time scale, a few centuries. These two results support the hibernation scenario of novae, which suggests that novae remain bright for a few centuries after eruption because of irradiation-induced mass transfer. After irradiation decreases mass transfer slows, and some (most?) very old novae may then become extremely faint.

Subject heading: stars: binaries — stars: late-type — stars: novae

I. INTRODUCTION

Eruptions of classical novae are truly spectacular events, detectable in external galaxies as distant as the Virgo Cluster (Pritchet and van den Bergh 1986). The underlying cause of a nova's great brilliance is believed to be a thermonuclear runaway (TNR) in the degenerate, hydrogen-rich envelope of a mass accreting white dwarf star in a close binary.

While the mechanism that powers novae is reasonably well understood, the long term evolution of these and related cataclysmic binaries is controversial. As basic a parameter as nova system lifetime has been estimated as 10^8 yr (Patterson 1984) to 10^{10} yr (Bath and Shaviv 1978; Shara *et al.* 1986). These uncertainties correspond to large uncertainties in the mass transfer rates $\dot{M}$ during the centuries or millenia between nova eruptions. Any physical understanding or meaningful modeling of nova binary evolution must include a correct prescription for $\dot{M}$. Most studies to date have assumed constant $\dot{M}$, but this and related papers (Shara *et al.* 1986; Livio and Shara 1987) emphasize that $\dot{M}$ may vary by orders of magnitude during several distinct phases between nova eruptions. A time-varying $\dot{M}$ yields TNRs and novae just like those generated by a constant $\dot{M}$ (Prialnik and Shara 1986). However, only for a time variable $\dot{M}$ can mass accretion rates as large as the commonly observed values $\dot{M} \sim 10^{-8}$ $M_\odot$ yr^{-1} yield TNRs violent enough to produce classical novae.

There is an aspect of nova evolution that has not yet been analyzed in detail, but that is crucial in determining $\dot{M}$ and the resulting appearance of a nova years or decades after eruption. This is the effect of fierce irradiation of the red dwarf by its adjacent, highly luminous white dwarf (but see MacDonald 1980). Of order 10^3 $L_\odot$ should fall on the red dwarf during the peak of the nova outburst and 10–100 $L_\odot$ for decades afterward. This is vastly more luminosity than the $\sim 10^{-1}$ $L_\odot$ typically produced by the secondaries in cataclysmics. We expect this irradiation to increase $\dot{M}$ greatly after an eruption, and a series of numerical simulations confirming this statement are the main thrust of this work. The method of computation, numerical treatment of irradiation and initial models are given in § II. The results of the simulations are described in § III, and the implied mass transfer rates are calculated in § IV. Implications for the hibernation scenario are discussed in § V. Our conclusions and summary are given in § VI.

II. THE METHOD OF COMPUTATION

a) The Binary Configuration

We consider a classical nova binary system whose primary is a 1.25 $M_\odot$ (M_1) white dwarf, and whose secondary (M_2) is a main-sequence star that fills its Roche lobe. The binary separation d is determined for given M_1 and M_2 by the requirement that the secondary's radius R_2 equal the effective radius of the Roche lobe r_L (Eggleton 1983).

When the primary undergoes a nova outburst, its luminosity ($L_{\rm nova}$) rises quickly to a plateau value of the order of the Eddington luminosity $L_{\rm E} \approx 4 \times 10^4$ $L_\odot$. The constant luminosity phase usually lasts for a few weeks, during which the erupting star sheds its envelope, and then $L_{\rm nova}$ slowly declines. According to the evolutionary calculations of Prialnik (1986), the variation of $L_{\rm nova}$, corresponding to a 1.25 $M_\odot$ progenitor, from the onset of the outburst ($t = 0$) onward, may be approximated by

$$L_{\rm nova} = \begin{cases} \dfrac{t}{t_1} L_{\rm Edd} \, , & 0 \le t < t_1 \, , \\ L_{\rm Edd} \, , & t_1 \le t < t_2 \, , \\ \left(\dfrac{t}{t_2}\right)^{-1.14} L_{\rm Edd} \, , & t \ge t_2 \, , \end{cases} \tag{1}$$

where $t_1 = 2 \times 10^4$ s and $t_2 = 3 \times 10^6$ s.

During this time the secondary is irradiated by the primary's radiation incident on its cross section:

$$L_{\rm irr} = \frac{\omega}{4\pi} L_{\rm nova} , \tag{2}$$

where ω is the solid angle given by

$$\omega/4\pi = (1 - \sin \theta)/2 , \tag{3}$$

with

$$\theta = \cos^{-1} (R_2/d) . \tag{3}$$

After t_2 the white dwarf's effective temperature is greater than 10^5 K, and its extreme ultraviolet radiation (EUV) will rapidly ionize the atmosphere of the secondary (facing the primary). This radiation should be converted to optical continuum photons at an optical depth inside the secondary of $\tau_{\rm EUV} \sim 1$. If we assume the energy of absorbed radiation to spread evenly over the surface of the secondary and consider a uniformly irradiated star, then an effective temperature of the irradiation T_s may be defined by the relation

$$L_{\rm irr} = 4\pi R_2^2 \sigma T_s^4 . \tag{5}$$

The validity of such an approximation has been considered by Edwards (1980), who showed that in a nonuniformly irradiated star horizontal streaming motions set in that should rapidly lead to uniform heating.

However, the detached, diskless binary system BE UMa (Ferguson *et al.* 1981; Margon, Downes, and Katz 1981) cautions that this approximation is simplistic. In BE UMa a low-mass M dwarf irradiated by a very hot ($T \approx 100{,}000$ K) white dwarf shows phase-dependent emission-line and optical continuum radiation. Both of these are maximal when the secondary is behind the white dwarf in the observer's line of sight, and minimal half an orbit later. (These effects are usually not seen in old classical novae where the accretion disk dominates the system light; Ferguson 1983). Thus the irradiated side of the secondary is hotter than the hemisphere facing away from the white dwarf. This will tend to increase the effective irradiation temperature by as much as 20% to $T_s = (L_{\rm irr}^2/2\pi R_2^2 \sigma)^{1/4}$ in equation (5), and increase the mass transfer rate $\dot{M}$ at a given epoch after eruption. The *qualitative* system behavior that we calculate in § III and § IV will be unchanged.

We then estimate the time scale for thermalization throughout the secondary's illuminated hemisphere by

$$\delta t_h \sim R_2/v_s \sim R_2/(R_G T_s/\mu)^{1/2} \sim 2 \times 10^4 \text{ s} , \tag{6}$$

where v_s is the sound velocity, R_G—the gas constant and μ is the mean molecular weight ($\mu = 1.25$). Thus δt_h is many orders of magnitude smaller than the *evolutionary* time scale of the illuminated secondary's outer envelope (estimated below at 10^9–10^{10} s) and our assumption of a uniform temperature T_s is justified.

The period of brightening of the nova (t_1), which is comparable to δt_h, is unimportant for the subsequent evolution of the secondary, and is assumed merely for numerical convenience. In fact, the phase of real significance from the point of view of the secondary's evolution is the phase of decline in the nova luminosity, which provides almost 90% of the energy output (since $\int_{t_2}^{\infty} L_{\rm nova}\, dt / \int_0^{t_2} L_{\rm nova}\, dt \approx 7$). This is fortunate, since our calculations assume that the radiation is provided to the secondary by a point source rather than by an extended star. Our assumption is valid for $t > 3 \times 10^6$ s, i.e., after the end of the mass-loss phase in the nova evolution. At this time the ejected shell has become transparent in the continuum and the declining nova luminosity is emitted from the surface of the white dwarf, which is close to being a point source ($R_{\rm WD} \ll d$). The parameters describing the binary configuration are listed in Table 1.

TABLE 1

PARAMETERS OF THE BINARY SYSTEM

$M_2/M_\odot$	q	r_L/d	$\omega/4\pi$	$\log (L_{\rm irr}/L_\odot)$[a]	$T_s/10^4$ K[a]
0.25.........	0.2	0.2517	0.0161	2.810	5.89
0.50.........	0.4	0.3031	0.0235	2.974	4.96
0.75.........	0.6	0.3357	0.0290	3.066	3.99

[a] Corresponding to $L_{\rm nova} = L_{\rm Edd}$.

b) The Boundary Conditions for a Uniformly Irradiated Star

To obtain the temperature distribution in the outer layers of the illuminated secondary as a function of the optical depth, namely $T(\tau)$, we consider a flux σT_s^4 incident on a semi-infinite medium. We seek a solution of the transfer equation that corresponds to a constant *net* flux F (either positive or negative), so that the emergent radiation is

$$L = L_{\rm irr} + 4\pi R_2^2 F . \tag{7}$$

In a state of thermal equilibrium, the star's configuration would adjust so as to support an outgoing flux equal to the sum of the incident flux and that generated within the star (i.e., "total reflection"); F would become $L_2/4\pi R_2^2$, where L_2 is the main-sequence luminosity of the secondary.

An approximation for $T(\tau)$ (after Milne 1930) is obtained by setting the Planck function

$$B(\tau) = a_1 - a_2 e^{-\tau} + a_3 \tau , \tag{8}$$

where the constants a_1, a_2, and a_3 are determined by requiring radiative equilibrium and correct flux at optical depth $\tau = 0$ and at great depths $\tau \to \infty$. This yields

$$\sigma T^4(\tau) = \left[\frac{3}{4}\tau + \frac{1}{4}\left(1 + \frac{1}{\ln 2}\right) - \frac{e^{-\tau}}{8 \ln 2}\right] F + \frac{1}{\ln 2} \times \left(1 - \frac{1}{2} e^{-\tau}\right) \sigma T_s^4 , \tag{9a}$$

which is used in the form

$$F = \sigma T^4(\tau) - 1.4427(1 - 0.5e^{-\tau})\sigma T_s^4/(0.75\tau + 0.61067 - 0.18034e^{-\tau}) \tag{9b}$$

to obtain L (eq. [7]) as a function of T_s and a known value of T at a given τ.

The impinging flux exerts an external pressure on the irradiated star. Thus, to obtain the total pressure p at small τ, we solve

$$\kappa\left(P_g + \frac{F}{c}\tau\right) = \kappa\left[p - \frac{4}{3c}\sigma T(\tau)^4 + \frac{F}{c}\tau\right] = rg , \tag{10}$$

where $\kappa = \kappa(p, T)$ is the opacity, P_g is the gas pressure, and g is the acceleration of gravity, together with equation (9).

TABLE 2

CHARACTERISTICS OF THE INITIAL MODELS

$M_2/M_\odot$	$R_2/R_\odot$	$\log(L_2/L_\odot)$	$\log(T_e)$	M_{CE}/M_2	$\log(T_c)$	$\log(\rho_c)$
0.25.........	0.246	−2.143	3.532	1.0	6.848	2.150
0.50.........	0.420	−1.584	3.556	0.563	6.913	1.851
0.75.........	0.718	−0.951	3.597	0.073	6.968	1.730

c) *The Evolutionary Code and Initial Models*

The evolutionary calculations were carried out by means of a Lagrangian, fully implicit hydrodynamic code. The code was updated in order to adapt it to regimes of low temperatures and relatively high densities, such as those prevailing in low-mass main-sequence stars. Thus, the equation of state took account of dissociation equilibria for hydrogen (H, H^+, H_2) and helium (He, He^+, He^{++}), as well as the first ionization stage for the next 14 most abundant elements in Allen's (1973) table of cosmic abundances. In regions of partial electron degeneracy, "pressure ionization" was taken into account through a correction to the free energy, as suggested by Eggleton *et al.* (1973).

We used Stellingwerf's fit to the opactiy (1975, Appendix D) for $7 \times 10^3 < T < 10^6$ K. At lower temperatures, opacities were taken from Alexander *et al.* (1983, Table 2).

The initial models were zero-age main-sequence stars of solar composition ($X = 0.73$, $Y = 0.25$, $Z = 0.02$) in thermal and hydrostatic equilibrium. Their main characteristics are given in Table 2. The masses were chosen so as to cover the range of secondary masses estimated for cataclysmic variables in general and classical novae in particular (e.g., Ritter 1984). In addition, each of the models represents a different class of main-sequence stars, according to its internal structure: the 0.25 $M_\odot$ model is fully convective, the 0.50 $M_\odot$ has a very extended convective envelope around a radiative core, while the 0.75 $M_\odot$ has only a shallow outer convective envelope. *A priori*, it is not obvious that these stars will respond to irradiation in the same way.

Finally, we note that in this initial, exploratory paper, we have not included the effects of mass accretion onto the white dwarf in determining the latter's luminosity. This feedback effect will increase the white dwarf luminosity over that due only to cooling, by a factor of (roughly) 50% (after the Eddington luminosity phase is completed). The resultant mass transfer rates and time scales will be slightly larger than the values calculated here, but the qualitative behavior should be unchanged.

III. RESULTS OF THE EVOLUTIONARY CALCULATIONS

Hydrodynamic calculations of the evolution of the three initial models with $M_2 = 0.25$, 0.50, and 0.75 $M_\odot$, respectively, were carried out for simulation intervals of several hundred years, corresponding in each case to a decline in the irradiation luminosity by about four orders of magnitude.

All three models expanded as soon as irradiation began, overcoming the pressure exerted by impinging radiation flux. At the peak of L_{irr}, radiation pressure was comparable to the gas pressure in the outer stellar layers. The expansion velocities attained were very small, orders of magnitude smaller than the local sound velocities. The models reached their maximum radii shortly after the end of the constant L_{irr} phase (i.e., ~ 0.1 yr), and then contracted slowly. *The return to within* 3×10^{-4} *of the original radii took place on time scales which increased with decreasing* M_2, *ranging from* ~ 100 *yr for* $M_2 = 0.75\ M_\odot$ *to* ~ 500 *yr for* $M_2 = 0.25\ M_\odot$..

The degree of expansion beyond the initial radius, namely the Roche lobe overflow, may be expressed by a parameter defined as.

$$x = (R - R_2)/R_2 \equiv (R - r_L)/r_L \ . \qquad (11)$$

The variation of x on a logarithmic time scale is given in Figure 1. Thus the smallest star underwent the largest relative expansion ($x_{max} = 1.8 \times 10^{-2}$) and overflowed its Roche lobe for the longest period of time. The evolutionary calculations were terminated in each case when $x < 10^{-4}$.

According to equation (9a), the extent in optical depth of the outer layer of a uniformly illuminated star that is affected by intense radiation may be estimated by equating the first term on the right-hand side (with the factor $F \sim L_2/4\pi R^2$) to the second term (with the factor of $\sigma T_s^4 \gg F$). At optical depths greater than $\tau_{irr} \sim L_{irr}/L_2$, the temperature distribution $T^4(\tau) \sim \frac{3}{4}\tau F$ is unaffected by L_{irr}. With the approximate relation

$$\tau_{irr} \approx \kappa\, \Delta m_{irr}/(4\pi R_2^2) \ , \qquad (12)$$

where Δm_{irr} is the mass of the affected layer, we obtain

$$\frac{\Delta m_{irr}}{M_2} \sim 10^{-10} \frac{L_{irr}}{L_2}\left(\frac{R_2}{R_\odot}\right)^2\left(\frac{M_2}{M_\odot}\right)^{-1}\left(\frac{\kappa}{\kappa_e}\right)^{-1} , \qquad (13)$$

where κ_e is the electron scattering opacity. In our case, the opacity changes by several orders of magnitude over a thin outer layer of the star, increasing from ~ 1 cm^2 g^{-1} near the surface up to 10^5 cm^2 g^{-1} and more in the hydrogen ionization zone. Thus only a crude *a priori* estimate $2 \times 10^{-11} < (\Delta m_{irr}/M_2) < 5 \times 10^{-7}$ is possible. *The numerical calculations yielded in all cases* $\Delta m_{irr}/M_2 \approx 5 \times 10^{-8}$.

In Figures 2*a*–2*c* temperature profiles as a function of mass are given for each of the three models, at different times during evolution. The high temperature of the illuminated surface results in a temperature inversion. An isothermal zone forms below the surface, whose extent increases gradually, as deeper layers of the star becomes affected by the irradiation flux. We emphasize that the rate of outward advection of material (see § IV) is competitive with the rate of inward flow of heat, and that Figures 2*a*–2*c* are only qualitatively indicative of the expected envelope thermal structures.

The variation with time of the isothermal region's temperature T_* and of the temperature of the irradiation flux T_s, is given in Figure 3 for the smallest and largest models, respectively. (The curves corresponding to the intermediate-mass model lie in between.) Two points are worthy of attention:

1. At all times $T_* > T_s$, as the outer region is heated both by the radiation flux incident at the surface, and by the outgoing energy flux from the interior of the star.

2. The evolution of T_* follows very closely that of T_s, meaning that the response time of the outer stellar layers to irradiation is very short, or equivalently, heating by the incident radiation is very efficient. This result is supported by a crude estimate of the heating (or response) time scale, as follows.

$$\delta t_r \sim \frac{R_G(T_s - T)\Delta m_{irr}}{\mu L_{irr}} \sim \frac{M_2 R_G T_s \Delta m_{irr}/M_2}{\mu L_{irr}} \sim 100 \text{ s} \ . \qquad (14)$$

The short δt_r provides further justification for the uniform irradiation approximation adopted in these calculations (see § II).

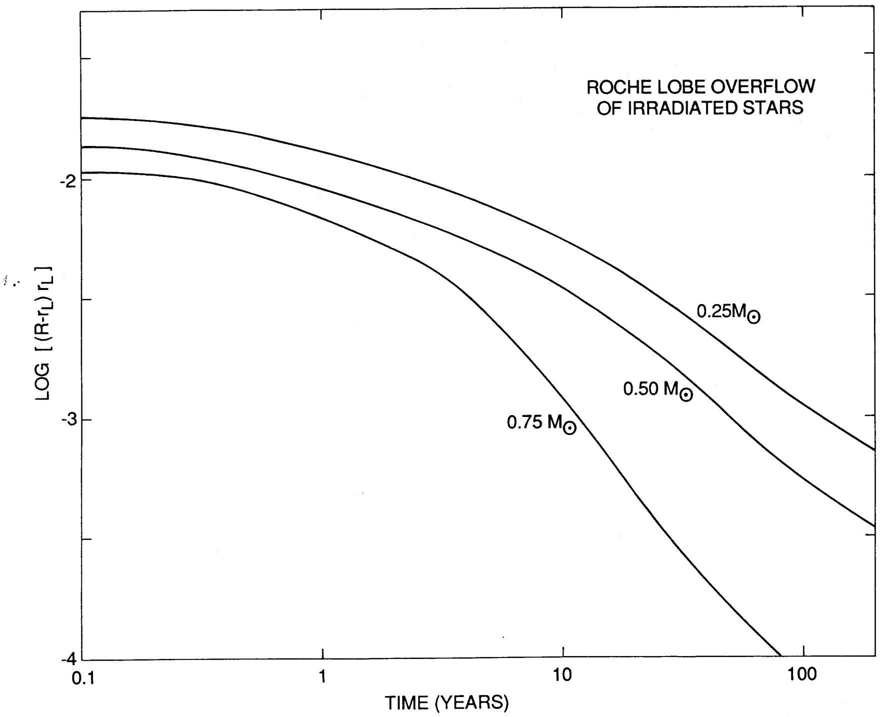

FIG. 1.—Variation of the Roche lobe overflow parmeter $x = (R - r_L)/r_L$ (eq. [11]) on a logarithmic time scale for the three models: 0.25 $M_\odot$, 0.50 $M_\odot$, and 0.75 $M_\odot$, as indicated, from the beginning of the nova decline ($t = t_2$, eq [1]) onward.

As the effect of irradiation reaches deeper into the star, the outer boundary of the convective zone recedes, as shown in Figure 4, so that convection starts below the outer isothermal zone. Only when the temperature inversion disappears, will convection gradually recover its lost ground. We find that the net flux F at the surface (eq. [9b]) is negative (i.e., into the star) so long as the irradiation luminosity is at its maximum—during the first 3×10^6 of the evolution—but changes sign and increases very slowly, as $L_{\rm irr}$ declines. The thermal equilibrium values $4\pi R_2^2 F = L_2$ is not attained during the first few hundred years of evolution, when $L_{\rm irr} \gg L_2$. The reason is that although $\Delta m_{\rm irr}$ is small, the corresponding thermal time scale

$$\delta t_{\rm th} \sim GM_2 \Delta m_{\rm irr}/R_2 L_2 \sim 10^{10} \text{ s} \tag{15}$$

is relatively long. Only when $L_{\rm irr}/\dot{L}_{\rm irr} \gtrsim \delta t_{\rm th}$ may we expect an equilibrium solution equivalent to total reflection. By this time, however, $L_{\rm irr}$ will have become of the order of L_2 and the effect of irradiation will have ceased to be significant.

The configurations of the initial models obey, on average, the relations $R_2 \propto M_2^{0.76}$ and $L_2 \propto M_2^3$. Since $\Delta m_{\rm irr}/M_2$ is approximately the same for all models, we obtain from equation (15):

$$\delta t_{\rm th}(M_2) \propto M_2^{-1.76} . \tag{16}$$

Thus equilibrium is expected to be regained on time scales that relate to each other as $\delta t_{\rm th}$ (0.75 $M_\odot$): $\delta t_{\rm th}$ (0.50 $M_\odot$): $\delta t_{\rm th}$(0.25 $M_\odot$) = 1:2:7. Indeed, the total evolutionary times, by the end of which the temperature distribution was close to the initial one, were 5.35×10^9 s, 1.37×10^{10} s, and 3.20×10^{10} s for the 0.75 $M_\odot$, 0.50 $M_\odot$, and 0.25 $M_\odot$ models, respectively.

IV. ESTIMATE OF THE MASS TRANSFER RATE

The results of our evolutionary calculations have shown that the expansion of the secondary upon irradiation is very nearly hydrostatic. The highest velocities attained were about two orders of magnitude lower than the sound velocity $v_s = (R_G T/\mu)^{1/2}$. In addition, as shown in Figure 2, the outer layers of the star, in particular those that have expanded beyond the initial radius, were isothermal.

The rate of mass flow $\dot{M}$ through the inner Lagrangian point (L_1) is proportional to the product of the velocity ($\sim v_s$), density ρ, and cross section of the stream Q:

$$\dot{M} \propto Q v_s \rho . \tag{17}$$

The effective cross section at L_1, as given by Meyer and Meyer-Hofmeister (1983), may be written in the form

$$Q = \eta\pi(v_s/\Omega)^2 , \tag{18}$$

where

$$\Omega = G(M_1 + M_2)/d^3 , \tag{19}$$

and the factor η depends on the Roche geometry. For all cases considered here $\eta \approx 0.2$.

The effective gravity at the surface of the secondary star in the vicinity of the Roche lobe radius r_L along the line of centers, may be approximated by

$$g(r \sim r_L) = (r - r_L) \left.\frac{dg}{dr}\right|_{r=r_L} = \frac{\alpha(r - r_L)GM_2}{r_L^3} , \tag{20}$$

where

$$\alpha = 2\left[1 + \frac{q^{-1}}{(d/r_L - 1)^3} + \frac{1}{2}\frac{(1 + q^{-1})}{(d/r_L)^3}\right] . \tag{21}$$

Using Paczyński's (1971) approximation

$$r_L/d = 0.46224[q/(1 + q)]^{1/3} , \tag{22}$$

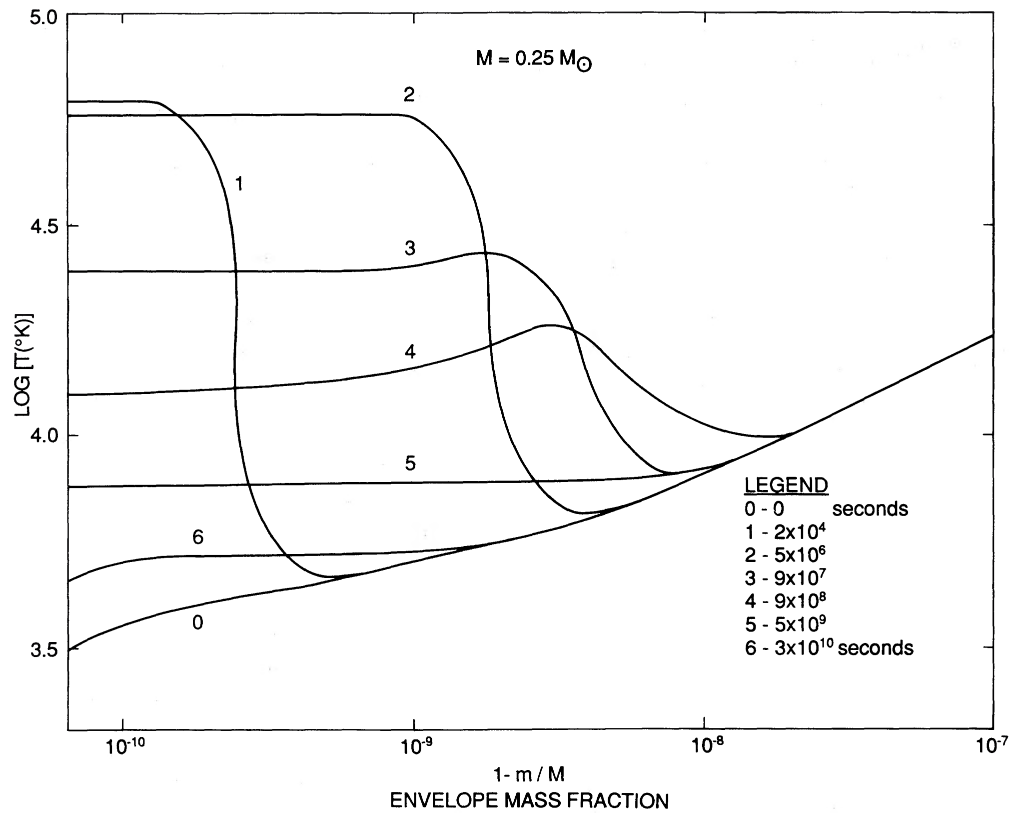

FIG. 2*a*

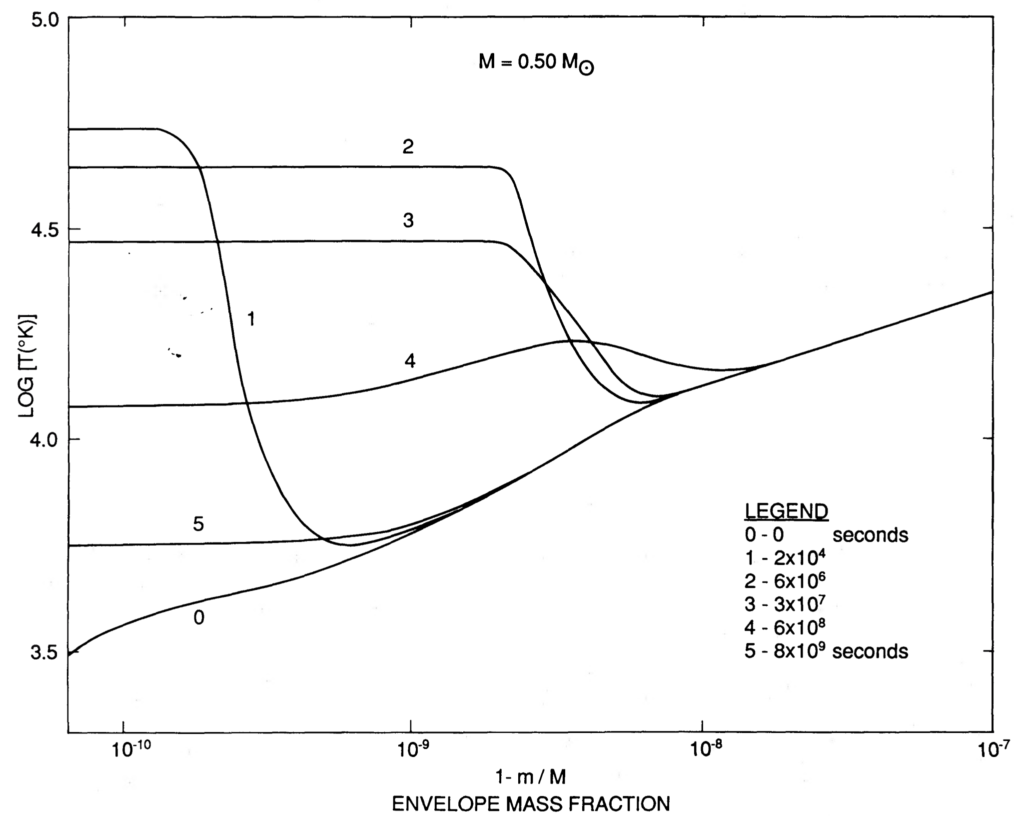

FIG. 2*b*

FIG. 2.—(*a*) Temperature profiles for the 0.25 $M_{\odot}$ model as a function of depth (in relative mass) below the surface, down to 10^{-7} of the total mass. Times (in seconds), are given corresponding to the different curves, labeled by integers. Curve marked "0" represents the initial, equilibrium model. (*b*) Same as (*a*), but for the 0.50 $M_{\odot}$ model. (*c*) Same as (*a*), but for the 0.75 $M_{\odot}$ model.

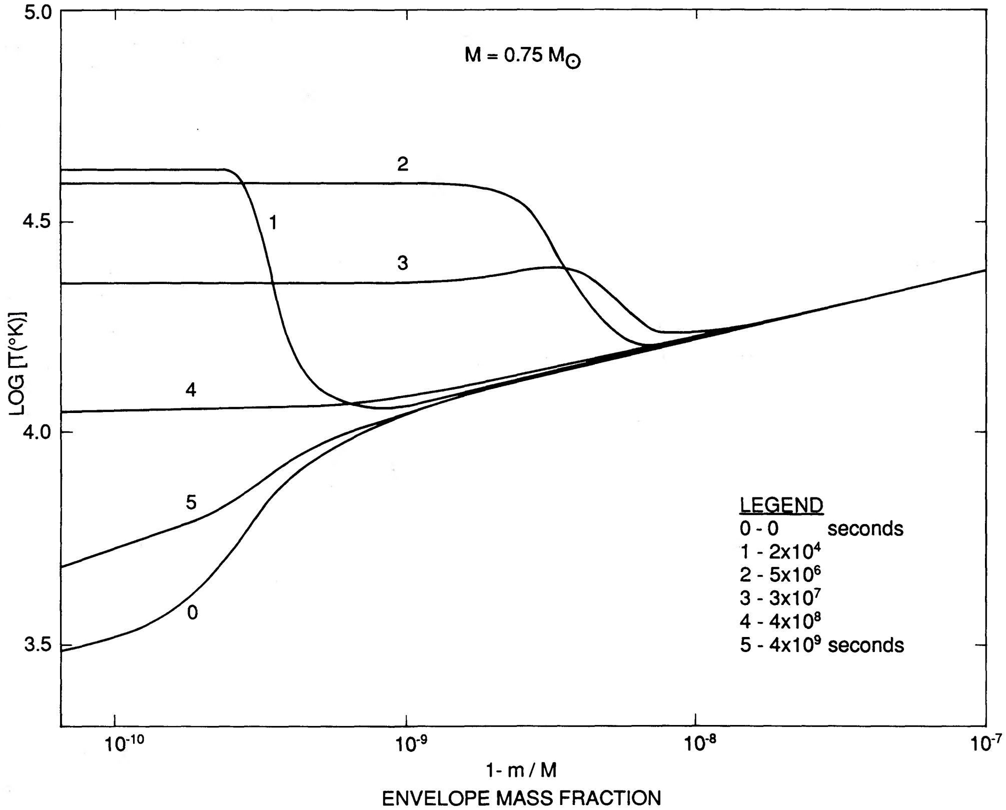

FIG. 2c

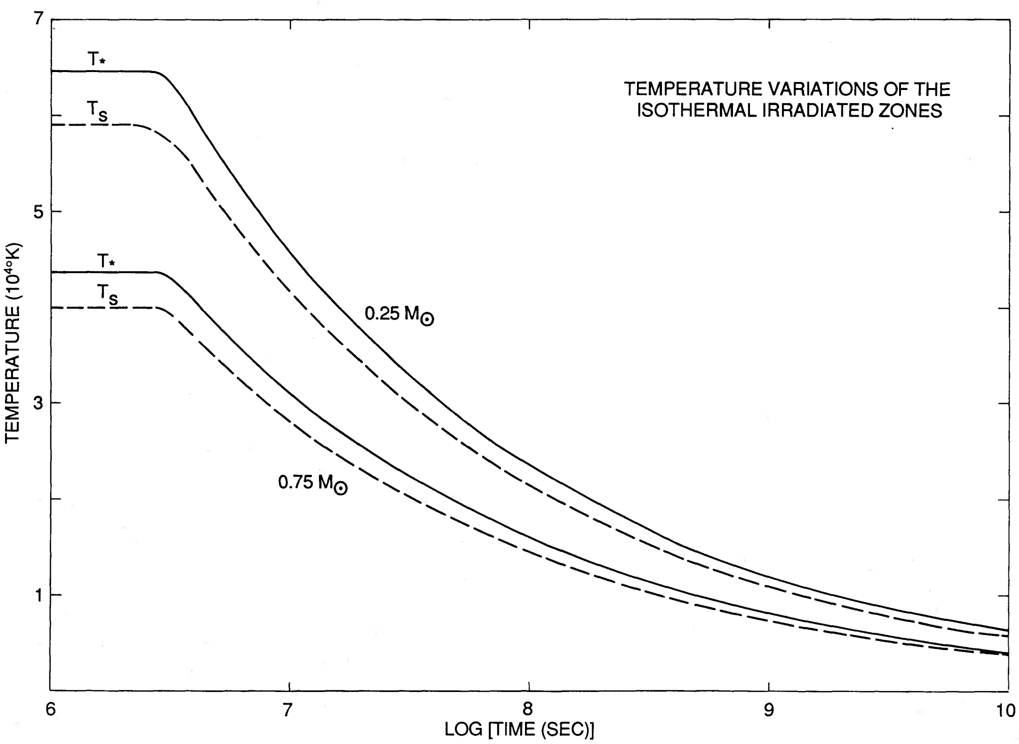

FIG. 3.—Variation with time of the temperature T_* of the isothermal outer region of the irradiated star, and of the temperature T_s of the corresponding irradiation flux (eq. [5]). Upper curves correspond to the 0.25 $M_\odot$ model, and lower ones to the 0.75 $M_\odot$ model.

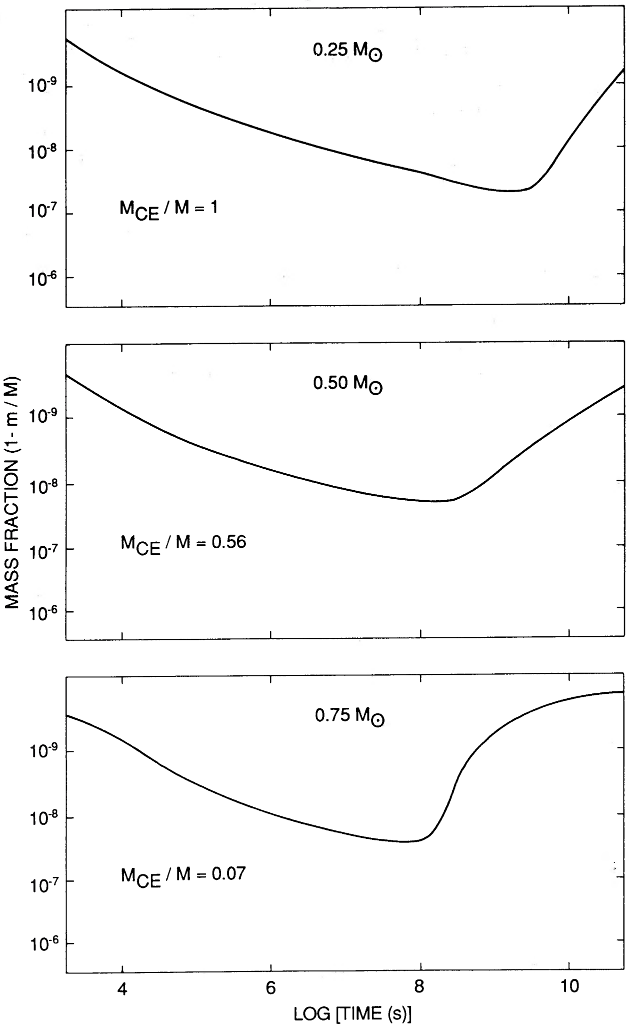

FIG. 4.—Variation with time of the outer boundary of the convective envelope for the three models. The mass of the convective envelope M_{CE} in the equilibrium models is given, relative to the total mass. The 0.25 $M_\odot$ model is fully convective in equilibrium.

which is accurate to within 1% in the range $0.1 < q < 1$ (see Eggleton 1983), we obtain $\alpha \approx 2.5$ for this range. Hence, by integrating the isothermal hydrostatic equation

$$\frac{1}{\rho}\frac{d\rho}{dx} = \frac{2.5}{v_s^2}\frac{GM_2}{r_L}x\ , \tag{23}$$

with x defined by equation (11), we obtain

$$\rho = \rho_0 \exp{(x/H)^2}\ , \tag{24}$$

where

$$H = \left(\frac{R_G T/\mu}{2.5GM_2/r_L}\right)^{1/2} \approx 0.016T_4^{1/2}\ , \tag{25}$$

and $T_4 = T/10^4$ K. As in § III, we set $r_L = R_2$ and take ρ_0 as the density below the photosphere ($\tau = \frac{2}{3}$) in the initial (Roche lobe filling) model.

Substituting equations (18) and (24) in equation (17), we finally obtain

$$\dot{M}(T_4, x) \propto \dot{M}_s T_4^{3/2} \exp{[(x/0.016)^2/T_4]}\ , \tag{26}$$

TABLE 3

MASS TRANSFER RATES ($M_\odot$ yr^{-1})

$M_2/M_\odot$	$\dot{M}_s$	$\dot{M}(x = x_{max})/\dot{M}(x = 10^{-4})$
0.25.........	2.3×10^{-8}	110
0.50.........	2.5×10^{-8}	82
0.75.........	3.2×10^{-8}	49

where

$$\dot{M}_s = 0.14(R_2/R_\odot)^3(M_2/M_\odot)^{-1}\rho_0 \tag{27}$$

is a constant, depending only on the structure of the secondary. Characteristic ratios of the mass transfer rate are given in Table 3. *$\dot{M}$ is typically two orders of magnitude higher at outburst maximum ($x = x_{max}$) than in quiescence ($x = 0$) a few centuries later.* The mass transfer rate was arbitrarily calibrated so as to correspond to $\dot{M} = 10^{-9}\ M_\odot$ yr^{-1} at $t = 100$ yr for the 0.5 $M_\odot$ model

The variation of $\dot{M}$ on a logarithmic time scale is given in Figure 5 for all three models. As the curves are close parallel straight lines to a very good accuracy, we find that

$$\frac{\dot{M}}{\dot{M}_0} = \left(\frac{t}{t_0}\right)^{-a}\ , \tag{28}$$

with $a \approx 0.45$, independent of the secondary's mass or radius. In fact, since the exponent in equation (26) varies only between 1 and 1.3 in the cases considered here, we expect $\dot{M}/\dot{M}_0 \sim T^{3/2} \sim T_s^{3/2} \sim L_{irr}^{3/8} \sim t^{-0.43}$.

While the numerical values of $\dot{M}$ at any time after eruption are uncertain, *the long-term trend of $\dot{M}$ is unmistakably clear: $\dot{M}$ decreases by orders of magnitude on a time scale of centuries.*

V. IRRADIATION AND THE HIBERNATION SCENARIO

Low observed space densities (e.g., Downes 1986) and high mass transfer rates (decades after eruption) in novae which have erupted early this century (Robinson 1975) imply short nova lifetimes. However, the two oldest recovered novae (CK Vul 1670 and WY Sge 1783) are much fainter than novae that have erupted this century (Shara and Moffat 1982, 1983; Shara, Moffat, and Webbink 1985; Shara *et al.* 1984), implying that mass transfer can decrease dramatically a few centuries after an outburst. If this happens to many novae then system lifetimes could be 10^{10} yr. The results of § IV strongly support variable $\dot{M}$ scenarios. Indeed, we maintain that it is difficult to defend a constant $\dot{M}$ hypothesis in light of these results.

The hibernation scenario describes the following cyclic behavior of many nova systems (though not all—Livio and Shara 1987). Mass is accreted at a high rate ($\sim 10^{-8}\ M_\odot$ yr^{-1}) for $\sim 10^3$ yr until an outburst occurs. Most of the white dwarf's hydrogen-rich envelope is ejected in weeks or months. The white dwarf's outer layers remain very hot for $\sim 10^2$ yr, irradiating the companion red dwarf and keeping mass transfer high ($\sim 10^{-8}$–$10^{-9}\ M_\odot$ yr^{-1}) as observed in the posteruptive novae of this century. The present work supports this part of the scenario.

The effects of systematic mass loss during a nova eruption on the binary parameters are such that the separation between the red and white dwarfs will *increase* in most cases (Shara *et al.* 1986). This leads to the secondary underfilling its Roche lobe and *significantly reducing mass transfer* (*a state of "hibernation") once irradiation from the erupting white dwarf becomes unimportant.* Gravitational radiation and/or magnetic

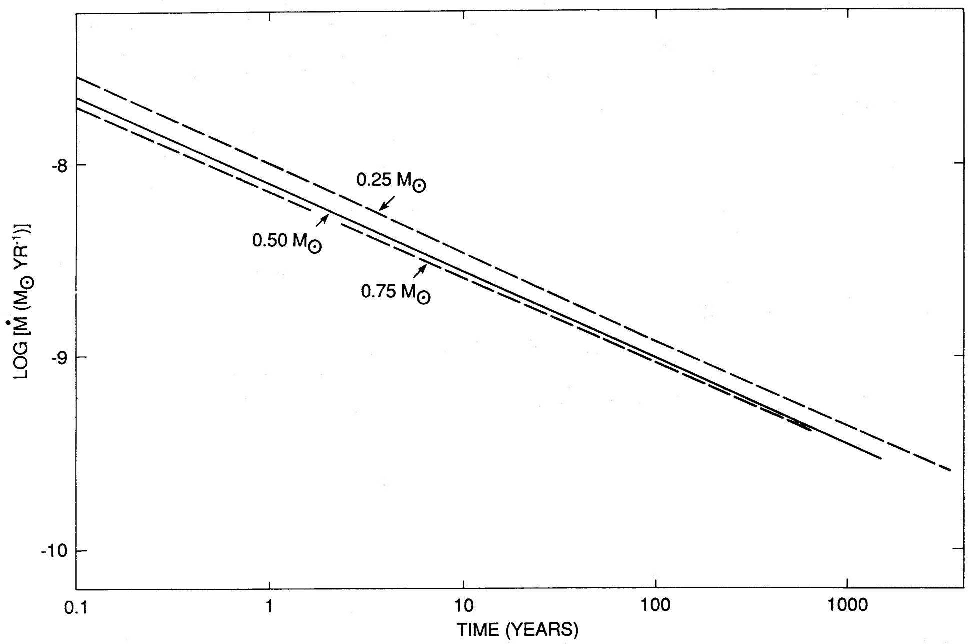

FIG. 5.—Estimated mass transfer rate $\dot{M}$ ($M_\odot$ yr^{-1}) from the illuminated secondary to the primary with $T = T(t)$ and $x = x(t)$, for each of the three models, from $t = t_2$ until it has contracted back to its initial radius (i.e., $x = 0$). The proportionality factor in eq. (26) was chosen so as to yield $\dot{M}$ (t = 100 yr) = 10^{-9} $M_\odot$ yr^{-1} for the 0.5 $M_\odot$ model.

braking eventually reduce the separation to its initial value, and mass transfer resumes. Only if hibernation lasts for at least 10^3 yr is the subsequent thermonuclear runaway violent enough to produce a nova (Prialnik and Shara 1986). (At least 10^3 yr are needed for the material accreted right after the eruption to cool, become degenerate, and diffuse into the white dwarf carbon-oxygen core). Much of the envelope mass necessary for a TNR is then accreted at high $\dot{M}$ in the last few centuries before eruption. This is why most prenovae appear as bright as postnovae (in the context of the hibernation scenario).

Finally, we note that the heretofore puzzling, extraordinary faintness of nova Cygni 1975 now appears to have been explained in a manner consistent with the hibernation scenario. V1500 Cygni is a polar (Kaluzny and Semeniuk 1987; Schmidt, Smith, and Elston 1987). This clearly links polars and novae and supports the hibernation scenario philosophy of metamorphosis between the various kinds of cataclysmic binaries.

The white dwarf's strong magnetic field almost certainly inhibits the rate at which is can accrete mass. Because a high $\dot{M}$ phase in the centuries before eruption was precluded, the prenova appeared extremely faint ($B \gtrsim 21$). This low $\dot{M}$ state can also be thought of as hibernation. The processes emphasized by Prialnik and Shara (1986) (i.e., degeneracy and Z enhancements) become increasingly important as the interval of low $\dot{M}$, prenova evolution is increased. If V1500 Cygni is forced by the white dwarf's strong magnetic field to always have low $\dot{M}$, then its very powerful eruption is seen to be a logical consequence of its long, magnetically enforced hibernation.

VI. SUMMARY AND CONCLUSIONS

We can briefly summarize our work as follows:

1. An erupting nova subjects its red dwarf companion to irradiation far in excess of the companion's own luminosity for many decades.

2. This irradiation causes the red dwarf's outer layers to expand by up to 2% and overflow the star's Roche surface. As irradiation decreases, so does the red dwarf's expansion.

3. A simple model of the resultant mass transfer shows that $\dot{M}$ drops by two orders of magnitude during the centuries following eruption.

4. These findings support the view that mass transfer decreases strongly in cataclysmic binaries long after eruption. If the "hibernation" scenario of novae is correct, then centuries or millenia of low or near-zero $\dot{M}$ may occur. The scenario explains how high observed $\dot{M}$ systems succeed in producing thermonuclear runaways (degeneracy and Z enrichment occurs during hibernation); the apparent low space densities of cataclysmics (many are hibernating much of the time); and suggests that at least some dwarf and classical novae metamorphosize into each other (as $\dot{M}$ rises or falls).

We thank Peter Stockman and Keith Horne for valuable criticisms and suggestions. D. P. thanks the Space Telescope Science Institute's Associates Program for generous support.

REFERENCES

Alexander, D. R., Johnson, H. R., and Rypma, R. L. 1983, *Ap. J.*, **272**, 773.
Allen, C. W. 1973, *Astrophysical Quantities*, (3d ed. London: Athlone).
Bath, G., and Shaviv, G. 1978, *M.N.R.A.S.*, **183**, 515.
Downes, R. 1986, *Ap. J.*, **307**, 170.
Edwards, A. C. 1980, *M.N.R.A.S.*, **190**, 757.
Eggleton, P. P. 1983, *Ap. J.*, **268**, 368.
Eggleton, P. P., Faulkner, J., and Flannery, B. P. 1973, *Astr. Ap.*, **23**, 325.
Ferguson, D. H. 1983, Ph.D. thesis, University of Arizona.
Kaluzny, J., and Semeniuk, I. 1987, preprint.
Livio, M., and Shara, M. M. 1987, *Ap. J.*, **319**, 819.

MacDonald, J. 1980, *M.N.R.A.S.*, **191**, 933.
Meyer, F., and Meyer-Hofmeister, E. 1983, *Astr. Ap.*, **121**, 29.
Milne, E. A. 1930, in *Handbuch der Astrophysik*, Vol. **3**, ed. G. Eberhard, A. Kohlschütter, and H. Lundendorff (Berlin: Springer), p. 65.
Paczyński, B. 1971, *Ann. Rev. Astr. Ap.*, **9**, 183.
Patterson, J. 1984, *Ap. J. Suppl.*, **54**, 443.
Prialnik, D. 1986, *Ap. J.*, **310**, 222.
Prialnik, D., and Shara, M. M. 1986, *Ap. J.*, **311**, 172.
Pritchet, C., and van den Bergh, S. 1986, preprint.
Ritter, H. 1984, *Astr. Ap. Suppl.*, **57**, 385.
Schmidt, G. D., Smith, P., and Elston, R. 1987, *IAU Circ.* No. 4415.
Shara, M. M., Livio, M., Moffat, A. F. J., and Orio, M. 1986, *Ap. J.*, **311**, 163.
Shara, M. M., and Moffat, A. F. J. 1982, *Ap. J. (Letters)*, **258**, L41.
———. 1983, *Ap. J.*, **264**, 560.
Shara, M. M., Moffat, A. F. J., McGraw, J. T., Dearborn, D. S., Bond, H. E., Kemper, E. and Lamontagne, R. 1984, *Ap. J.*, **282**, 763.
Shara, M. M., Moffat, A. F. J., and Webbink, R. F. 1985, *Ap. J.*, **294**, 286.
Stellingwerf, R. F. 1975, *Ap. J.*, **195**, 441.

ATTAY KOVETZ: School of Physics and Astronomy, and Department of Geophysics and Planetary Sciences, Raymond and Beverly Sackler Faculty of Exact Sciences, Tel Aviv University, Ramat-Aviv 69978, Israel

DINA PRIALNIK: Racah Institute of Physics, Hebrew University of Jerusalem, Jerusalem 91904, Israel

MICHAEL M. SHARA: Space Telescope Science Institute, 3700 San Martin Drive, Baltimore, MD 21218